Critical Vortex Shedding in a Strongly Interacting Fermionic Superfluid

Jee Woo Park,[1] Bumsuk Ko,[1,2] and Y. Shin[1,2,*]
[1]Department of Physics and Astronomy, and Institute of Applied Physics, Seoul National University, Seoul 08826, Korea
[2]Center for Correlated Electron Systems, Institute for Basic Science, Seoul 08826, Korea

(Received 22 May 2018; published 28 November 2018)

We study the critical vortex shedding in a strongly interacting fermionic superfluid of ^{6}Li across the BEC-BCS crossover. By moving an optical obstacle in the sample and directly imaging the vortices after the time of flight, the critical velocity u_{vor} for vortex shedding is measured as a function of the obstacle travel distance L. The observed u_{vor} increases with decreasing L, where the rate of increase is the highest in the unitary regime. In the deep Bose-Einstein condensation regime, an empirical dissipation model well captures the dependence of u_{vor} on L, characterized by a constant value of $\eta = -[d(1/u_{\mathrm{vor}})/d(1/L)]$. However, as the system is tuned across the resonance, a step increase of η develops about a characteristic distance L_c as L is increased, where L_c is comparable to the obstacle size. This bimodal behavior is strengthened as the system is tuned towards the BCS regime. We attribute this evolution of u_{vor} to the emergence of the underlying fermionic degree of freedom in the vortex-shedding dynamics of a Fermi condensate.

DOI: 10.1103/PhysRevLett.121.225301

Superfluidity, the absence of friction in a particle flow, is a spectacular demonstration of macroscopic quantum coherence. One of its defining properties is the existence of a critical velocity, above which the creation of fundamental excitations gives rise to drag and dissipation in the superfluid. From a microscopic perspective, the Landau criterion presents a critical velocity $v_{\mathrm{LD}} = \min_p[\epsilon(p)/p]$, where $\epsilon(p)$ is the energy of the superfluid's microscopic excitation with momentum p. However, it is known that, when a superfluid flows past an obstacle larger than the healing length ξ, the nucleation of quantized vortices lowers the critical velocity below v_{LD} [1] and that their creation strongly modifies the thermodynamic and transport response of the superfluid [2,3]. Despite their importance, the details of the vortex nucleation process and its relation to the superfluid's microscopic modes of excitation remain as open questions, in particular, in the study of strongly correlated quantum fluids [4–6].

Strongly interacting atomic Fermi gases with tunable interactions offer an interesting opportunity to investigate the microscopic aspects of superfluid dissipation by accessing the crossover between Bose-Einstein condensation (BEC) and Bardeen-Cooper-Schrieffer (BCS) superfluidity [7–14]. In the crossover, the nature of superfluidity changes from bosonic to fermionic, and the elementary excitation determining the Landau criterion is transformed from phonons to fermionic pair-breaking excitations [15]. Superfluid dissipation in the BEC-BCS crossover has been explored in a number of experiments, where the critical velocity for heating in the presence of a moving obstacle or in a counterflow of bosonic and fermionic superfluids was measured [16–18], and, recently, the emergence of dissipation in a Josephson junction by phase slip and vortex nucleation was studied [19,20]. However, the roles of the coexisting elementary excitations and their possible interplay in the nucleation of quantized vortices remain obscure.

In this Letter, we report on the measurement of the critical velocity u_{vor} for vortex shedding in a strongly interacting fermionic superfluid of ^{6}Li across the BEC-BCS crossover. The response of the superfluid to a pulsed linear motion of an obstacle over a finite distance L results in a characteristic dependence of u_{vor} on L. A general tendency for u_{vor} to increase with decreasing L, which is expected from energy considerations, is observed for all investigated interaction strengths. However, the maximal rate of increase is observed near unitarity, implying that Fermi superfluidity is the most robust in this regime. In the BEC limit, we find that the characteristic relationship between u_{vor} and L is described by a constant value of $\eta = -[d(1/u_{\mathrm{vor}})/d(1/L)]$, which is in accordance with an empirical model that assumes a linear dependence of the dissipation rate on the obstacle velocity. In the crossover regime, however, we observe a sudden jump of η at a characteristic distance L_c as L is increased, where L_c is comparable to the obstacle size, and this jump becomes larger when approaching the BCS regime. We argue that this evolution is attributable to the emergence of the fermionic nature of superfluidity in the BEC-BCS crossover. Our results shed light on the role of the microscopic excitations in a superfluid's vortex nucleation dynamics and also provide a stringent benchmark for time-dependent theories of strongly interacting fermionic systems [21–23].

The experiment starts with the creation of a strongly interacting fermionic superfluid of ^{6}Li in an optical dipole trap. To this end, the experimental apparatus described in

Ref. [24] has been modified to accommodate ^{6}Li together with bosonic ^{23}Na. In the experiment, both species are simultaneously loaded into a magneto-optical trap and then optically pumped and transferred into a plugged magnetic quadrupole trap, where forced radio-frequency (rf) evaporation of ^{23}Na sympathetically cools ^{6}Li to quantum degeneracy [25,26]. The resulting ^{6}Li atoms are then loaded into an optical dipole trap formed by focusing a 1064 nm laser beam.

To access the strongly interacting regime, we use a broad s-wave Feshbach resonance between the two lowest hyperfine states of ^{6}Li (denoted $|1\rangle$ and $|2\rangle$) located at 832 G, which allows precise tuning of the s-wave scattering length a [27]. Initially, all the atoms are transferred to $|1\rangle$, and then an equal mixture of the two states is prepared near 860 G using Landau-Zener rf sweeps. The final stage of evaporation is performed at 815 G by reducing the dipole trap laser intensity. After evaporation, the magnetic field is adiabatically ramped to a value where the critical velocity measurement will be performed. At unitarity, this procedure produces a superfluid sample consisting of $N \approx 1.0 \times 10^6$ ^{6}Li atoms per spin state with a typical condensate fraction of approximately 80%, corresponding to a temperature of $T/T_F < 0.1$ [28]. Here, $T_F = E_F/k_B$ is the Fermi temperature, where $E_F = \hbar^2 k_F^2/2m = \hbar\bar{\omega}(6N)^{1/3}$ is the Fermi energy of a noninteracting Fermi gas, $\hbar$ is the reduced Planck constant, k_F is the Fermi wave number, m is the atomic mass of ^{6}Li, and $\bar{\omega}$ is the geometric mean of the trap frequencies. The final trapping frequencies are $(\omega_x, \omega_y, \omega_z) = 2\pi \times (17, 18, 483)$ Hz, where the radially symmetric confinement is mainly provided by the residual magnetic field curvature from the Feshbach field and the tight z confinement is provided by the optical dipole trap.

A schematic of the experiment is shown in Fig. 1(a). A repulsive optical obstacle is translated through the center of the sample by a fixed distance L during a variable time t at a constant velocity $u = L/t$. After the sweep, the Feshbach field is switched off, and simultaneously the sample is released from the trap for time-of-flight expansion, during which the vortices expand radially to allow detection within our optical resolution. Following the expansion, an absorption image of the condensate is taken at $B = 690$ G [26]. A representative set of images displaying one and two generated vortex dipoles are shown in the inset in Fig. 1(c). The critical velocity for vortex shedding is extracted from a sigmoidal fit to the probability $P(u)$ of observing vortex-antivortex pairs as $P(u) = 1/(1 + e^{-(u-u_{\rm vor})/\sigma})$, where $P(u)$ is obtained by varying the time t for a given L [Fig. 1(c)].

The repulsive optical obstacle consists of a focused 532 nm Gaussian laser beam propagating along the z axis, whose position is controlled using a piezoactuated mirror [29]. The $1/e^2$ radius of the beam is $w_0 = 9.5$ μm, which is an order of magnitude larger than the Fermi length scale $1/k_F \approx 0.30$ μm. The height of the obstacle is set at

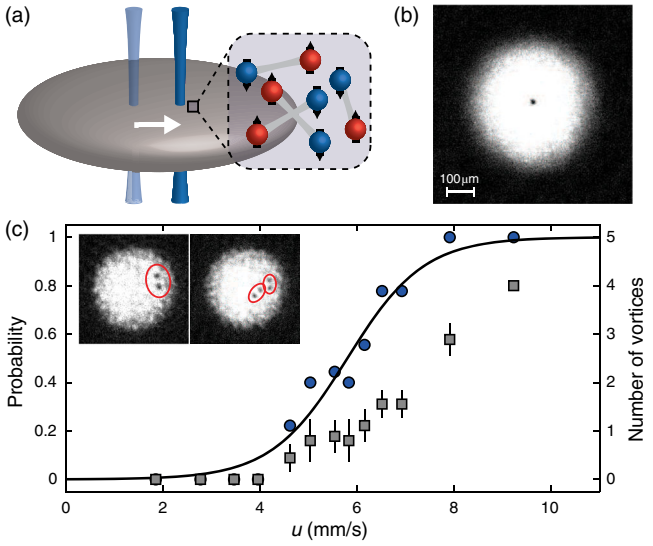

FIG. 1. Vortex shedding in a strongly interacting fermionic superfluid. (a) Schematic of the experiment. A cylindrical impenetrable obstacle, consisting of a focused repulsive Gaussian laser beam, is translated at a constant velocity through the center of a disk-shaped strongly interacting fermionic condensate of ^{6}Li. (b) An *in situ* image of the condensate at unitarity penetrated by the obstacle. (c) The number of vortices (gray squares) and the probability of observing vortex dipoles (blue circles) after sweeping the obstacle as a function of u. The shown data set is obtained at unitarity with $L = 27.7$ μm using the quick obstacle switch-off procedure [26]. Each data point comprises at least nine realizations of the same experiment. The black solid line is a sigmoidal fit to the probability. From the fit, $u_{\rm vor}$ is extracted by setting $P(u_{\rm vor}) = 1/2$.

$k_B \times 10$ μK, which is about 20 times higher than the Fermi energy $E_F \approx k_B \times 0.45$ μK. Comparing the obstacle height to the chemical potential of the sample, the obstacle has an effective diameter of $D \approx 26$ μm at unitarity [26,29]. The radial Thomas-Fermi radius $R_{{\rm TF},r}$ of the sample at unitarity is 260 μm, which is significantly larger than the obstacle sweeping distance L ranging from 20 to 90 μm. $R_{{\rm TF},z}$ in the z direction (12 μm) is much shorter than the Rayleigh length of the obstacle beam (590 μm), ensuring its negligible divergence within the condensate.

When employing the obstacle beam, precaution is taken to avoid exciting unwanted dynamics in the condensate. To this end, we apply sufficient intensity ramp times and hold times before and after the obstacle translation. Their effects on the measured critical velocities are studied, and the values are carefully chosen to be independent of the measurements [26].

The vortex-shedding critical velocities for various sweeping distances are measured for a broad range of interaction strengths covering the BEC-BCS crossover, as shown in Fig. 2. As a reference, the speed of sound $v_{s,{\rm exp}}$ of the superfluid is also measured from the propagating speed of an outgoing circular density wave, which is triggered by abruptly switching off the obstacle beam depleting the

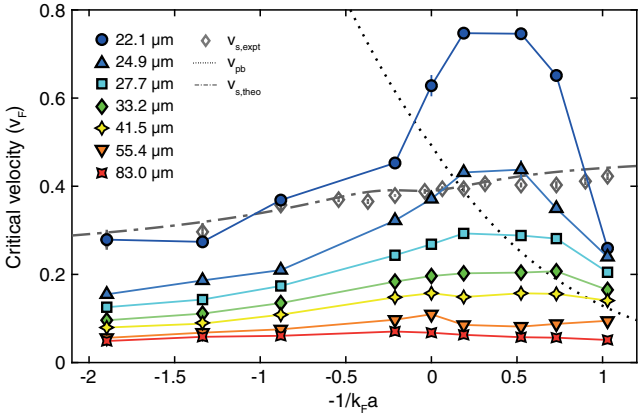

FIG. 2. The measured critical velocity for vortex shedding u_{vor} (filled markers) at different sweeping lengths L and the speed of sound $v_{s,\mathrm{exp}}$ (open diamonds) in the BEC-BCS crossover, in units of the Fermi velocity v_F. The error bars for u_{vor} and $v_{s,\mathrm{exp}}$ represent one standard deviation of the sigmoidal fit to $P(u)$ and the linear fit to the density wave propagation, respectively. The unseen error bars are hidden by the markers. The gray dot-dashed line is the theoretical speed of sound $v_{s,\mathrm{theo}}$ from quantum Monte Carlo calculations, for column-averaged densities [31]. The black dotted curve is the pair-breaking velocity v_{pb} from the mean-field BCS theory.

center of the sample [17,26,30]. This is shown together with a theoretical speed of sound $v_{s,\mathrm{theo}}$ for the column-averaged density from quantum Monte Carlo calculations [31,32] and the mean-field BCS pair-breaking velocity v_{pb}. Since our sample is hydrodynamic in the z axis, $v_{s,\mathrm{exp}}$ should be determined by the column-averaged density. Here, the theory curves are scaled to our definition of k_F using the equation of state while assuming the local density approximation.

The most notable feature in Fig. 2 is the dramatic increase of u_{vor} near unitarity as the sweeping distance L is reduced. The rise of u_{vor} with decreasing L is expected, in general, since the necessary energy for vortex nucleation has to be provided within a shorter obstacle travel distance. The enhanced rate of increase near unitarity reflects the stability of superfluidity in this regime, which is consistent with previous experiments that reported the maximal robustness of fermionic superfluidity near unitarity [16,17,19,20]. However, a comparison between u_{vor} and $v_{\mathrm{LD}} = \min(v_s, v_{\mathrm{pb}})$ must be made prudently, since u_{vor} probes the vortex nucleation dynamics within a finite distance L, whereas v_{LD} signifies the onset of dissipation via the creation of microscopic excitations [15–17]. One may conjecture that u_{vor} will converge to v_{LD} for infinitely long L, where a scaling factor determined by the obstacle geometry may be involved.

Another surprise comes from the observation of well-defined vortex-shedding critical velocities exceeding the speed of sound for sufficiently short L. When an object moves through a medium faster than its speed of sound, shock waves are created that lead to strong density modulations. Furthermore, the ensuing flow will be turbulent, and vortex shedding will be highly irregular [22,33]. Thus, it is out of expectation that no abrupt change in the response of u_{vor} is observed when the obstacle is translated faster than the speed of sound over a short distance. In fact, this behavior is observed throughout the explored crossover regimes when L is sufficiently reduced (red data points in Fig. 3), suggesting that it may be a general characteristic of a compressible gaseous superfluid.

To further elucidate the dependence of u_{vor} on L, we adopt a simple dissipation model where an obstacle moving faster than the critical velocity for the appearance of a drag

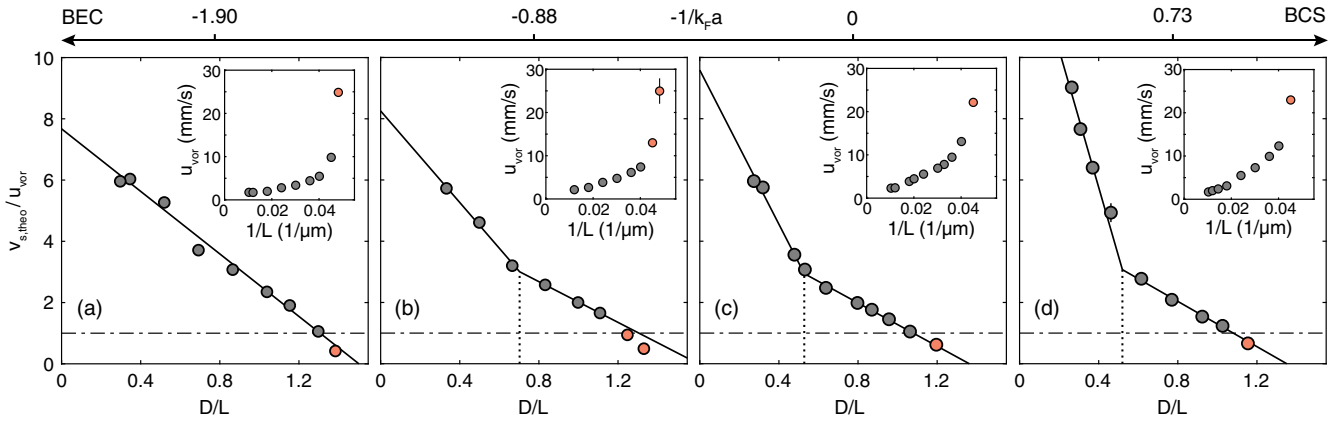

FIG. 3. Inverse critical velocity $1/u_{\mathrm{vor}}$ as a function of the inverse sweeping distance $1/L$. u_{vor} and L are normalized by the speed of sound $v_{s,\mathrm{theo}}$ and the effective obstacle diameter D, respectively. Four representative graphs whose $-1/k_F a$ is equal to (a) -1.9, (b) -0.88, (c) 0, and (d) 0.73 are shown. The solid line is the fit of the dissipation model to the data points with $u_{\mathrm{vor}} < v_{s,\mathrm{theo}}$ (gray) while excluding those with $u_{\mathrm{vor}} > v_{s,\mathrm{theo}}$ (red). The dotted line indicates the characteristic D/L_c where the bimodality develops. The dot-dashed line marks where $u_{\mathrm{vor}} = v_{s,\mathrm{theo}}$. The error bars are one standard deviation of the fit. The insets show the values of u_{vor} as a function of $1/L$.

force, u_c^0, deposits energy into the system at a rate given by $P = \Gamma(u - u_c^0)$ [29,34,35]. Here, Γ is a proportionality constant that captures the energy transfer efficiency. When the energy cost of exciting a vortex dipole is E_c, we have $E_c = Pt = \Gamma(u_{\rm vor} - u_c^0)(L/u_{\rm vor})$, which can be reexpressed as

$$u_{\rm vor}(L) = \frac{u_c^0}{1 - l_0/L}, \tag{1}$$

where $l_0 = E_c/\Gamma$. Note that l_0 denotes the minimum distance required to shed a vortex dipole. This model motivates us to plot the inverse of $u_{\rm vor}$ versus $1/L$ for each interaction strength, as shown in Fig. 3. Here, $u_{\rm vor}$ and L are normalized with respect to the speed of sound $v_{s,\rm theo}$ and the obstacle diameter D at each $1/k_F a$, respectively. We find that the model fits the data exceptionally well in the far BEC regime [Fig. 3(a)], where the change of $u_{\rm vor}$ with L is characterized by a constant magnitude of the slope, $\tilde{\eta} = \eta \times v_{s,\rm theo}/D$. We note that our measurements indicate $u_c^0 = 0.13 v_{s,\rm theo}$, which is about 3 times lower than the previous result obtained for a weakly interacting BEC with a highly oblate geometry [29,36]. This discrepancy may arise from the stronger three-dimensional nature of our sample [33,37].

Approaching the resonance, however, the experimental data deviate from the model, showing a sudden jump of $\tilde{\eta}$ near $L_c \sim 1.5D$ as L is increased. This bimodal structure emerges already on the BEC side near the Feshbach resonance and becomes further pronounced as the interaction is tuned towards the BCS regime. We characterize this evolution by applying a bilinear fit to the data while excluding the data points with $u_{\rm vor} > v_{s,\rm theo}$, as shown in Figs. 3(b)–3(d). The fitted values of L_c/D exhibit a slightly increasing trend towards the BCS limit [Fig. 4(a)], and the ratio of $\tilde{\eta}$ in the long $L > L_c$ branch to that in the short $L < L_c$ branch increases by up to almost an order of magnitude as $1/k_F a$ approaches -1 [Fig. 4(b)].

The y intercept of the fit represents the inverse of the critical velocity for the appearance of drag, u_c^0, at the investigated interaction strength, and we compare the obtained u_c^0 with the Landau critical velocity $v_{\rm LD} = \min(v_s, v_{\rm pb})$ [15–17]. We find that the overall trend of u_c^0 closely follows $v_{\rm LD}$ in the BEC-BCS crossover, as shown in Fig. 4(c), which suggests that the onset of the drag force leading to vortex dipole emission is strongly affected by the microscopic degrees of freedom of the superfluid. Specifically, the suppression of $u_c^0/v_{s,\rm theo}$ towards the BCS regime reveals the participation of the pair-breaking energy scale in the vortex-shedding dynamics across the crossover.

It is remarkable that $\tilde{\eta}$ for short $L < L_c$ is nearly constant at the value established in the far BEC regime throughout the crossover [Fig. 4(b)]. Since the superfluid's fermionic characteristics are negligible in the BEC regime, this

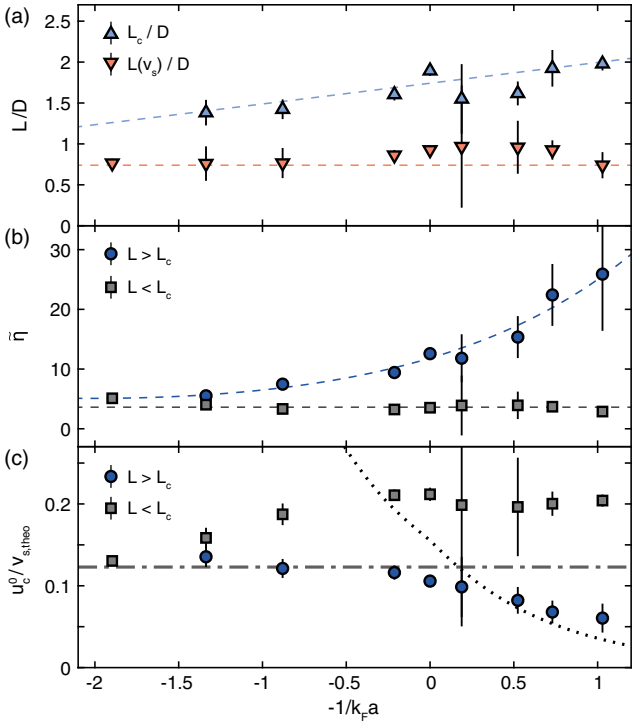

FIG. 4. Characterization of the evolution of $u_{\rm vor}(L)$ in the BEC-BCS crossover. (a) The sweeping distance L_c at which a step jump of $\tilde{\eta}$, the magnitude of the slope of the fit, is observed (blue triangles), and the value of L where $u_{\rm vor} = v_{s,\rm theo}$ (inverted red triangles). The dashed lines are guides to the eye. (b) $\tilde{\eta}$ for $L > L_c$ (blue circles) and $L < L_c$ (gray squares). The blue and gray dashed lines are a guide to the eye. (c) The inverse of the y intercept of the fit, equal to the critical velocity for drag normalized by the speed of sound, for $L > L_c$ (blue circles) and $L < L_c$ (gray squares). The speed of sound (dot-dashed line) and the pair-breaking velocity (dotted line) normalized by the speed of sound with a multiplicative factor are shown together. The error bars are one standard deviation of the fit.

observation may suggest that the vortex nucleation dynamics is governed by the speed of sound in the short L branch, even away from the BEC limit. Looking closely, however, if we linearly extrapolate the data with $L < L_c$ and extract the critical velocity $u_c^0(L < L_c)$, its value increases with respect to the speed of sound until it reaches a plateau around the resonance [Fig. 4(c)], showing that the nucleation of vortices for short $L < L_c$ cannot be explained solely by the speed of sound.

Our measurements suggest the involvement of the pair-breaking mechanism in the vortex-shedding dynamics of a strongly interacting fermionic superfluid, but they pose a number of questions as to what determines the critical distance L_c and why the transition across L_c is so sharp. Furthermore, a description of the microscopic mechanism through which the gap energy scale enters the nucleation process remains to be clarified. A possible scenario is that the pair-breaking mechanism induces a local depletion of the superfluid, thereby lowering the critical velocity for

vortex nucleation. However, a further inquiry is necessary to understand the dynamical interplay between the bosonic and fermionic elementary excitations in the vortex nucleation process.

In conclusion, we have measured the critical velocity for vortex shedding and studied its dependence on the obstacle sweeping distance in a strongly interacting fermionic condensate across the BEC-BCS crossover. A steep increase of the critical velocity is observed near unitarity, demonstrating the robustness of Fermi superfluidity in this regime, and a characteristic transition in the vortex-shedding dynamics across the BEC-BCS crossover is revealed, suggesting the involvement of the pair-breaking excitations in the vortex-shedding dynamics. In light of the recent experimental observation of a von Kármán vortex street in a weakly interacting BEC [38], it would be intriguing to investigate the universality of the vortex-shedding behavior in the current system, e.g., in terms of L_c/D and l_0/D.

We thank Aurel Bulgac for helpful discussions. This work was supported by the Institute for Basic Science in Korea (Grant No. IBS-R009-D1) and the National Research Foundation of Korea (Grant No. NRF-2018R1A2B3003373). J. W. P. acknowledges support from the POSCO Science Fellowship of the POSCO TJ Park Foundation.

*yishin@snu.ac.kr

[1] R. J. Donnelly, *Quantized Vortices in Helium II* (Cambridge University Press, Cambridge, England, 1991).
[2] G. Blatter, M. V. Feigel'man, V. B. Geshkenbein, A. I. Larkin, and V. M. Vinokur, Rev. Mod. Phys. **66**, 1125 (1994).
[3] W. F. Vinen and J. J. Niemela, J. Low Temp. Phys. **128**, 167 (2002).
[4] P. W. Anderson, Rev. Mod. Phys. **38**, 298 (1966).
[5] A. Bulgac, M. M. Forbes, and P. Magierski, *BCS-BEC Crossover and the Unitary Fermi Gas*, Lect. Notes Phys. Vol. 836, edited by W. Zwerger (Springer, Berlin, 2011).
[6] E. Varoquaux, Rev. Mod. Phys. **87**, 803 (2015).
[7] M. Greiner, C. A. Regal, and D. S. Jin, Nature (London) **426**, 537 (2003).
[8] S. Jochim, M. Bartenstein, A. Altmeyer, G. Hendl, S. Riedl, C. Chin, J. H. Denschlag, and R. Grimm, Science **302**, 2101 (2003).
[9] M. W. Zwierlein, C. A. Stan, C. H. Schunck, S. M. F. Raupach, S. Gupta, Z. Hadzibabic, and W. Ketterle, Phys. Rev. Lett. **91**, 250401 (2003).
[10] C. A. Regal, M. Greiner, and D. S. Jin, Phys. Rev. Lett. **92**, 040403 (2004).
[11] M. W. Zwierlein, C. A. Stan, C. H. Schunck, S. M. F. Raupach, A. J. Kerman, and W. Ketterle, Phys. Rev. Lett. **92**, 120403 (2004).
[12] T. Bourdel, L. Khaykovich, J. Cubizolles, J. Zhang, F. Chevy, M. Teichmann, L. Tarruell, S. J. J. M. F. Kokkelmans, and C. Salomon, Phys. Rev. Lett. **93**, 050401 (2004).
[13] C. Chin, M. Bartenstein, A. Altmeyer, S. Riedl, S. Jochim, J. Denschlag, and R. Grimm, Science **305**, 1128 (2004).
[14] M. W. Zwierlein, A. Schirotzek, C. H. Schunck, and W. Ketterle, Nature (London) **435**, 1047 (2005).
[15] R. Combescot, M. Y. Kagan, and S. Stringari, Phys. Rev. A **74**, 042717 (2006).
[16] D. E. Miller, J. K. Chin, C. A. Stan, Y. Liu, W. Setiawan, C. Sanner, and W. Ketterle, Phys. Rev. Lett. **99**, 070402 (2007).
[17] W. Weimer, K. Morgener, V. P. Singh, J. Siegl, K. Hueck, N. Luick, L. Mathey, and H. Moritz, Phys. Rev. Lett. **114**, 095301 (2015).
[18] M. Delehaye, S. Laurent, I. Ferrier-Barbut, S. Jin, F. Chevy, and C. Salomon, Phys. Rev. Lett. **115**, 265303 (2015).
[19] G. Valtolina, A. Burchianti, A. Amico, E. Neri, K. Xhani, J. A. Seman, A. Trombettoni, A. Smerzi, M. Zaccanti, M. Inguscio, and G. Roati, Science **350**, 1505 (2015).
[20] A. Burchianti, F. Scazza, A. Amico, G. Valtolina, J. A. Seman, C. Fort, M. Zaccanti, M. Inguscio, and G. Roati, Phys. Rev. Lett. **120**, 025302 (2018).
[21] A. Bulgac, Y. L. Luo, P. Magierski, K. J. Roche, and Y. Yu, Science **332**, 1288 (2011).
[22] F. Ancilotto, L. Salasnich, and F. Toigo, Phys. Rev. A **87**, 013637 (2013).
[23] M. M. Forbes and R. Sharma, Phys. Rev. A **90**, 043638 (2014).
[24] M.-S. Heo, J. Y. Choi, and Y. Shin, Phys. Rev. A **83**, 013622 (2011).
[25] Z. Hadzibabic, S. Gupta, C. A. Stan, C. H. Schunck, M. W. Zwierlein, K. Dieckmann, and W. Ketterle, Phys. Rev. Lett. **91**, 160401 (2003).
[26] See Supplemental Material at http://link.aps.org/supplemental/10.1103/PhysRevLett.121.225301 for further details on sample preparation, obstacle preparation and translation, and measurement of the speed of sound.
[27] G. Zürn, T. Lompe, A. N. Wenz, S. Jochim, P. S. Julienne, and J. M. Hutson, Phys. Rev. Lett. **110**, 135301 (2013).
[28] Q. Chen, J. Stajic, and K. Levin, Phys. Rev. Lett. **95**, 260405 (2005).
[29] W. J. Kwon, G. Moon, S. W. Seo, and Y. Shin, Phys. Rev. A **91**, 053615 (2015).
[30] J. Joseph, B. Clancy, L. Luo, J. Kinast, A. Turlapov, and J. E. Thomas, Phys. Rev. Lett. **98**, 170401 (2007).
[31] N. Manini and L. Salasnich, Phys. Rev. A **71**, 033625 (2005).
[32] G. E. Astrakharchik, J. Boronat, J. Casulleras, and S. Giorgini, Phys. Rev. Lett. **93**, 200404 (2004).
[33] T. Winiecki, B. Jackson, J. F. McCann, and C. S. Adams, J. Phys. B **33**, 4069 (2000).
[34] T. Frisch, Y. Pomeau, and S. Rica, Phys. Rev. Lett. **69**, 1644 (1992).
[35] T. Winiecki, J. F. McCann, and C. S. Adams, Phys. Rev. Lett. **82**, 5186 (1999).
[36] W. J. Kwon, S. W. Seo, and Y. Shin, Phys. Rev. A **92**, 033613 (2015).
[37] B. Jackson, J. F. McCann, and C. S. Adams, Phys. Rev. A **61**, 051603 (2000).
[38] W. J. Kwon, J. H. Kim, S. W. Seo, and Y. Shin, Phys. Rev. Lett. **117**, 245301 (2016).